Metal–Insulator Transition in the Hubbard Model on a Triangular Lattice with Disorders: Renormalization Group Approach

J. X. WANG, SABRE KAIS

Department of Chemistry, Purdue University, West Lafayette, IN 47907

ABSTRACT: A multistages block renormalization group approach to study the metal–insulator transition in the Hubbard model on a triangular lattice with hexagonal blocks is presented and implemented. A second-order phase transition with a critical point at $U/t = 12.5$ is obtained (the coupling parameters U and t correspond to the repulsive charging energy and to the nearest-neighbor exchange coupling terms, respectively). In the presence of disorder the phase diagram for the system exhibits a metallic phase, an insulating phase, and a domain-localized phase that separates them in the Mott regime. The subtle influence of electron–electron interactions upon inverse participation rate in the Anderson regime is also investigated. The results are discussed in light of experimental evidence for arrays of metalic quantum dots and exact numerical diagonalization of the Hubbard Hamiltonian. © 2003 Wiley Periodicals, Inc. Int J Quantum Chem 93: 360–374, 2003

Key words: Hubbard model; renormalization group; quantum dot; phase transition

1. Introduction

Two-dimensional arrays with tailored electronic properties are generating much current experimental and theoretical interest [1, 2]. This was made possible by the development of synthetic methods for the preparation of, so-called, quantum dots (QDs). There is much current interest in the ability to engineer nanoscale electronic devices, including quantum computers [3] from QDs.

QDs of nearly identical sizes self-assemble into a planar array. (The dots are passivated against collapse by coating them with organic ligands.) For, e.g., Ag nanodots, the packing is hexagonal. The lower-lying electronic states of an isolated dot are discrete, being determined by the confining potential (and therefore the size) of the dot. There is, however, one essential difference: Because of their larger size (100–1000 atoms each) it takes only a

Correspondence to: S. Kais; e-mail: kais@power1.chem.purdue.edu

relatively low energy to add another electron to a dot, as revealed by scanning tunneling microscopy [4]. This energy is much lower than the corresponding energy for ordinary atoms and most molecules. It follows that when dots are close enough to be exchange coupled, which is the case in an array, the charging energy, that is, the energy difference between the two configurations . . . DDDD . . . and . . . DD⁻D⁺D . . . , can be low. We here propose and implement a computational method that allows the contributions of such ionic configurations even for extended arrays. The technical problem is that the Coulombic repulsion between two electrons (of opposite spins) that occupy the same dot cannot be described in a one-electron approximation. It requires allowing for correlation of electrons. Most methods that explicitly include correlation effects scale as some high power of the number of atoms (here, dots) and are computationally intractable [5]. For example, a hexagonal array of only 19 dots, 3 dots per side, has already 2,891,056,160 low electronic configurations. So, earlier [6] exact computations including charging energy were limited to a hexagonal array of only seven dots, two dots per side. Yet, current measurements of both static [7] and transport [8] properties use arrays of at least 100 dots per side. The simplest Hamiltonian that includes both the Coulombic (or charging energy) effects and the exchange coupling is the Hubbard model [9]. This model can be solved exactly for a 1-D chain [10, 11]. But, for a 2-D array it is, so far, analytically intractable. In the absence of a closed solution, various methods have been developed. These include exact diagonalization methods [12], quantum Monte-Carlo simulations [13], and approximation techniques like mean-field theory [14], Green's function decoupling schemes [15], functional integral formulations [16], variational approach [17], and perturbation expansion [18]. Renormalization group (RG) methods are receiving increasing attention because of the nonperturbative nature, which allows application to the intermediate-to-strong coupling regime. In this direction, we have the density matrix renormalization group (DMRG) method [19], which provides a powerful new way to obtain reliable results for the 1-D Hubbard model, and the numerical renormalization group method for interacting finite Fermi systems and for excitations in atoms [20, 21]. For DMRG, efforts are now being made to apply it to 2-D cases. This article reports the applications of another kind of RG method, i.e., real-space block renormalization

group (BRG) method [22–25], to the Mott metal–insulator transition, a 2-D lattice [26–28].

Section 2 presents the real-space RG method and the RG equations for a fermion system on a triangular lattice with hexagonal blocks. By using an operator transformation, we then obtain the conditions for a renormalized Hubbard Hamiltonian having the same structure as the original one. In other words, the RG procedures retain the same coupling terms but with a renormalized strength. Then, by solving the RG equations numerically, one can determine the critical value for a Mott metal–insulator transition in this system to be $U/t = 12.5$. Experimentally prepared metallic QDs are not uniform in size. The best current efforts result in a size distribution with a width of about 6 nm [8] but it may be possible to do better in the future. As pointed out early in [29, 30] and emphasized since [2, 31], these fluctuations in size have a decisive influence on the electronic states of the array. All three coupling constants in the Hubbard Hamiltonian, Eq. (1) below, are modified by the size fluctuations. First, because size determines the confining potential the higher electronic states of each dot and hence the chemical potential of the dot, μ, in Eq. (1), can fluctuate. This is an important effect related to the filling of the lattice but we will not further discuss it here although we hope to return to it in the future. What concerns us is the half-filled system. And, we will investigate instead the site–energy fluctuation, which is considered by the Hubbard–Anderson Model. The MIT caused by site–energy disorder is known as Anderson MIT. In our work, we will focus upon the competitions between the disorder and the electron interactions in the electron localization effect. Next, the strength of the exchange coupling can fluctuate. It can do so for two reasons: Its range scales with the size of the dot [29, 32] and the packing disorder induced by the variable size. In Section 3 we examine the role of variation in the strength of the exchange coupling. We also examine the effect of variation in the charging energy U. (In the simplest picture, U is determined by the capacity of the dot and so scales inversely with its size.) The phase diagram for a system with disorder shows a mixed phase, intermediate between metallic and insulating. That there should be such a disorder-induced phase has been previously suggested [33, 34] and has also been seen experimentally in both static and transport measurements [2, 7]. These experiments were, however, for fairly compressed lattices, for which the

exchange coupling is strong and its effects overwhelm the role of the charging energy.

2. Real-Space Renormalization Group

2.1. GENERAL PROCEDURES

This section presents a general computational procedure for applying the BRG method for interacting fermions on a lattice using the Hubbard Hamiltonian. As an example we will take the hexagonal block on a triangular lattice. The Hubbard Hamiltonian is written as

$$H = -t \sum_{i,j,\sigma}' [c_{i\sigma}^+ c_{j\sigma} + \text{H.c.}]$$
$$+ U \sum_i n_{i\uparrow} n_{i\downarrow} - \mu \sum_i (n_{i\uparrow} + n_{i\downarrow}), \quad (1)$$

where t is the nearest-neighbor hopping (exchange coupling) term, U is the local repulsive interaction, and μ is the chemical potential. $c_{i\sigma}^+ (c_{i\sigma})$ creates (annihilates) an electron with spin σ in the valence orbital of the dot located at site i; the corresponding number operator is $n_{i\sigma} = c_{i\sigma}^+ c_{i\sigma}$. The prime on the first sum in Eq. (1) indicates that summation is restricted to nearest-neighbor dots. H.c. denotes the Hermitian conjugate. Note that this model Hamiltonian allows only one orbital per dot. That orbital can be empty or it can accommodate one or two electrons. U is the repulsion of two electrons (of opposite spins) placed in the same dot.

The essence of the BRG method is to map the above many-particle Hamiltonian on a lattice to a new one with fewer degrees of freedom and with the same low-lying energy levels [35]. Then, the mapping is repeated, leading to a final Hamiltonian for which an exact solution can be obtained. The procedure can be summarized into three steps: First divide the N-site into appropriate n_s-site blocks labeled by $p(p = 1, 2, \ldots, N/n_s)$ and separate the Hamiltonian H into intrablock part H_B and interblock H_{IB}

$$H = H_B + H_{IB} = \sum_p H_p + \sum_{\langle p,p' \rangle} V_{p,p'}, \quad (2)$$

where

$$H_p = -t \sum_{\langle i^{(p)}, j^{(p)} \rangle} [c_{i^{(p)}\sigma}^+ c_{j^{(p)}\sigma} + \text{H.c.}] + U \sum_{i^{(p)}} n_{i^{(p)}\uparrow} n_{i^{(p)}\downarrow}$$
$$- \mu \sum_{i^{(p)}} (n_{i^{(p)}\uparrow} + n_{i^{(p)}\downarrow}), \quad (3)$$

and

$$V_{p,p'} = -t \sum_{\langle i^{(p,b)}, j^{(p',b)} \rangle} [c_{i^{(p,b)}\sigma}^+ c_{j^{(p',b)}\sigma} + \text{H.c.}], \quad (4)$$

in which $i^{(p)}$ denotes the ith site on the pth block and $i^{(p,b)}$ denotes the border site of the block p.

The second step is to solve H_p exactly to get the eigenvalues E_{p_i} and eigenfunctions $\Phi_{p_i}(i = 1, 2, \ldots, 4^{n_s})$. Then, we can build the eigenfunctions of H_B by direct multiplication of Φ_{p_i}, which can be written as

$$|\Psi_B(i_1, i_2, \ldots, i_{N/n_s}) > = |\Phi_{1i_1}\rangle |\Phi_{2i_2} > \cdots |\Phi_{N/n_s i_{N/n_s}}$$
$$> (i_1, i_2, \cdots \in \{1, 2, \ldots, 4^{n_s}\}). \quad (5)$$

The last step is to treat each block as one site on a new lattice and the correlations between blocks as hopping interactions. The original Hilbert space has four states per site. By following the above procedure one obtains an equivalent Hamiltonian with $(4^{n_s})^{N/n_s} = 4^N$ degrees of freedom, which is the same as the original Hamiltonian. However, if we are only concerned with lower-lying states of the system it is not necessary to keep all the states for a block to obtain the new Hamiltonian. For example, when studying the metal–insulator transition [36] we may only need to consider the ground-state and the first excited-state energies.

2.2. RG EQUATIONS WITHOUT PROLIFERATIONS OF COUPLING PARAMETERS

The above scheme is a general procedure for applying the BRG method. To make the new Hamiltonian more tractable, it is desirable to make it have the same structure as the original one, i.e., the reduction in size should not be accompanied by a proliferation of new couplings. Then, we can use the iteration procedures to solve the model. To achieve this goal it is necessary to keep only four states in step 2, which can be understood from the following renormalized intrasite Hamiltonian. The four selected states are taken to be

$$|\Phi_{p1}\rangle \equiv |0\rangle_p', \quad (6)$$

TABLE I
Product of different operator transformations.

	$\langle 0|'$	$\langle \uparrow |'$	$\langle \downarrow |'$	$\langle \uparrow\downarrow |'$
$|0\rangle'$	$1 - n'_\uparrow - n'_\downarrow + n'_\uparrow n'_\downarrow$	$c'_\uparrow - n'_\downarrow c'_\uparrow$	$c'_\downarrow - n'_\uparrow c'_\downarrow$	$c'_\downarrow c'_\uparrow$
$|\uparrow\rangle'$	$c'^+_\uparrow - c'^+_\uparrow n'_\downarrow$	$n'_\uparrow - n'_\uparrow n'_\downarrow$	$c'^+_\uparrow c'_\downarrow$	$- n'_\uparrow c'_\downarrow$
$|\downarrow\rangle'$	$c'^+_\downarrow - c'^+_\downarrow n'_\uparrow$	$c'^+_\downarrow c'_\uparrow$	$n'_\downarrow - n'_\downarrow n'_\uparrow$	$n'_\downarrow c'_\uparrow$
$|\uparrow\downarrow\rangle'$	$c'^+_\uparrow c'^+_\downarrow$	$- n'_\uparrow c'^+_\downarrow$	$c'^+_\uparrow n'_\downarrow$	$n'_\uparrow n'_\downarrow$

The product reads $|0\rangle'\langle 0|' = 1 - n'_\uparrow - n'_\downarrow + n'_\uparrow n'_\downarrow$, etc.

$$|\Phi_{p2}\rangle \equiv c'^+_{p\uparrow\downarrow}|0\rangle'_p = |\uparrow\downarrow\rangle'_p, \tag{7}$$

$$|\Phi_{p3}\rangle \equiv c'^+_{p\uparrow}|0\rangle'_p = |\uparrow\rangle'_p, \tag{8}$$

$$|\Phi_{p4}\rangle \equiv c'^+_{p\uparrow}|0\rangle'_p = |\downarrow\rangle'_p, \tag{9}$$

where $c'^+_{p\sigma}(c'_{p\sigma})$ is the creation (annihilation) operator of the block state $|\sigma\rangle'_p$ and their corresponding energies are E_i ($i = 1, 2, 3, 4$).

Our next task is to rewrite the old Hamiltonian $H = H_B + H_{IB}$ in the space spanned by the truncated basis

$$H' = \sum |\Psi_B^T\rangle\langle\Psi_B^T|H|\Psi_B^T\rangle\langle\Psi_B^T|, \tag{10}$$

where the truncated basis is given by

$$|\Psi_B^T(i_1, i_2, \ldots, i_{N/n_s})\rangle = |\Phi_{1i_1}\rangle|\Phi_{2i_2}\rangle \cdots |\Phi_{N/n_s}i_{N/n_s}$$

$$> (i_1, i_2, \cdots \in \{1, 2, 3, 4\}). \tag{11}$$

To avoid proliferation of additional couplings in H', the four states kept from the block cannot be arbitrarily chosen. Some definite conditions must be satisfied to make H' have the same structure as H. Substituting H into H' and using the product of different operators (see Table I) we can get the expression for H_p

$$H_p = |0\rangle'_p E_1\langle 0|'_p + |\uparrow\downarrow\rangle'_p E_2\langle\uparrow\downarrow|'_p$$
$$+ |\downarrow\rangle'_p E_4\langle\downarrow|'_p + |\uparrow\rangle'_p E_3\langle\uparrow|'_p$$
$$= E_1 + (E_3 - E_1)n'_{p,\uparrow} + (E_4 - E_1)n'_{p,\downarrow}$$
$$+ (E_1 + E_2 - E_3 - E_4)n'_{p,\uparrow}n'_{p,\downarrow}. \tag{12}$$

Note that by keeping only four states from the block states in the beginning gives no extra couplings in the new Hamiltonian.

Comparing the above intrasite Hamiltonian with Eq. (1), we get the next conditions to copy the intrasite structure of the old Hamiltonian, i.e., $E_3 =$

E_4. Because of the additional vacuum energy E_1 in the new Hamiltonian we rewrite the intrasite part of Eq. (1) as

$$H_B = U \sum_i n_{i\uparrow}n_{i\downarrow}$$

$$- \mu \sum_i (n_{i\uparrow} + n_{i\downarrow}) + K \sum_i I_i, \tag{13}$$

where we introduce another parameter K to the original system and I_i is a unit operator. The new intrasite Hamiltonian is given by

$$H'_B = (E_1 + E_2 - 2E_3) \sum_p n'_{p\uparrow}n'_{p\downarrow}$$

$$- (E_1 - E_3) \sum_p (n'_{p\uparrow} + n'_{p\downarrow}) + E_1 \sum_p I_p. \tag{14}$$

Then, the renormalized parameters U, μ, and K can be obtained from the following relations:

$$U' = E_1 + E_2 - 2E_3, \tag{15}$$

$$\mu' = E_1 - E_3, \tag{16}$$

$$K' = E_1, \tag{17}$$

in which E_1, E_2, and E_3 are functions of the old parameters t, U, μ, K.

For the half-filled case, $\mu = U/2$, H_B can be expressed as

$$H_B = U \sum_i \left(\frac{1}{2} - n_{i\uparrow}\right)\left(\frac{1}{2} - n_{i\downarrow}\right) + K \sum_i I_i, \tag{18}$$

with the initial value of $K = -(U/4)$. By using the particle–hole symmetry, $E_1 = E_2$, the renormalization group equations for U and K take the form

$$U' = 2(E_1 - E_3), \qquad (19)$$

$$K' = (E_1 + E_3)/2. \qquad (20)$$

To illustrate this procedure, let us consider the triangular lattice with hexagonal blocks as shown in Figure 1. For this nonbipartite lattice the interaction between blocks can be written as

$$V_{pp'} = (-t) \sum_{\sigma, i_1, i'_1, i_2, i'_2} \{[|\Phi_{pi_1}\rangle\langle\Phi_{pi_1}|c^+_{1(p)\sigma}|\Phi_{pi'_1}\rangle\langle\Phi_{pi'_1}|]$$

$$\times [|\Phi_{p'i_2}\rangle\langle\Phi_{p'i_2}|c_{5(p')\sigma}|\Phi_{p'i'_2}\rangle\langle\Phi_{p'i'_2}|]$$

$$+ [|\Phi_{pi_1}\rangle\langle\Phi_{pi_1}|c^+_{2(p)\sigma}|\Phi_{pi'_1}\rangle\langle\Phi_{pi'_1}|]$$

$$\times [|\Phi_{p'i_2}\rangle\langle\Phi_{p'i_2}|c_{4(p')\sigma}|\Phi_{p'i'_2}\rangle\langle\Phi_{p'i'_2}|]$$

$$+ [|\Phi_{pi_1}\rangle\langle\Phi_{pi_1}|c^+_{2(p)\sigma}|\Phi_{pi'_1}\rangle\langle\Phi_{pi'_1}|]$$

$$\times [|\Phi_{p'i_2}\rangle\langle\Phi_{p'i_2}|c_{5(p')\sigma}|\Phi_{p'i'_2}\rangle\langle\Phi_{p'i'_2}|] + \text{H.c.}\}. \qquad (21)$$

Because we would like to keep $V_{pp'}$ of the form

$$V_{pp'} = (-t') \sum_\sigma [c'^+_{p\sigma}c'_{p'\sigma} + \text{H.c.}], \qquad (22)$$

we use the product transformation in Table I to simplify Eq. (20):

$$V_{pp'} = \sum_{\sigma,\langle i,j\rangle} \{\langle\sigma|'_p c^+_{i(p)\sigma}|0\rangle'_p + [\langle-\sigma, \sigma|'_p c^+_{i(p)\sigma}| - \sigma\rangle'_p$$
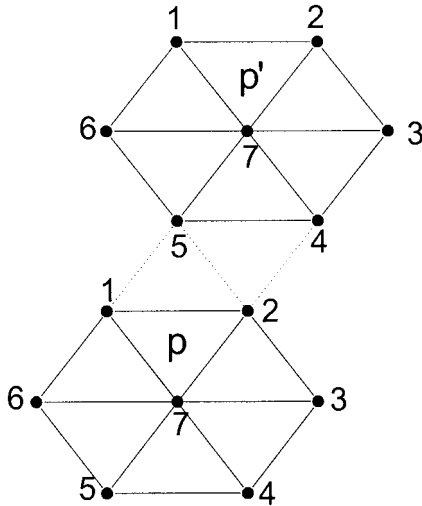

FIGURE 1. Schematic diagram of the triangular lattice with hexagonal blocks. Only two neighboring blocks p and p' are drawn here. The dotted lines represent the interblock interactions and the solid lines the intrablock couplings.

$$- \langle\sigma|'_p c^+_{i(p)\sigma}|0\rangle'_p]n'_{p-\sigma}\}c'^+_{p\sigma} \times \{\langle0|'_{p'}c_{j(p')\sigma}|\sigma\rangle'_{p'}$$

$$+ [\langle-\sigma, \sigma|'_{p'}c_{j(p')\sigma}|\sigma, -\sigma\Uparrow\rangle'_{p'}$$

$$- \langle\sigma|'_{p'}c_{j(p')\sigma}|0\rangle'_{p'}]n'_{p'-\sigma}c'_{p'\sigma} + \text{H.c.},$$

$$(\langle ij\rangle = \langle1, 5\rangle, \langle2, 4\rangle, \langle2, 5\rangle). \qquad (23)$$

It can be easily seen now that to make all the extra couplings vanish it is necessary to make further restrictions upon the selected states:

$$\langle-\sigma, \sigma|'_p c^+_{i(p)\sigma}| - \sigma\rangle'_p = \langle\sigma|'_p c^+_{i(p)\sigma}|0\rangle'_p, \qquad (24)$$

$$\langle-\sigma, \sigma|'_{p'}c_{j(p')\sigma}|\sigma, -\sigma\rangle'_{p'} = \langle0|'_{p'}c_{j(p')\sigma}|\sigma\rangle'_{p'}. \qquad (25)$$

Using similar calculations to the other neighboring interactions of the block, we can finally obtain the following conditions:

$$\langle-\sigma, \sigma|'_p c^+_{i(p)\sigma}| - \sigma\rangle'_p = \langle\sigma|'_p c^+_{i(p)\sigma}|0\rangle'_p = \lambda \qquad (26)$$

for all the border sites on the block. Then, the new hopping term becomes

$$V_{pp'} = \nu\lambda_2 \sum_\sigma c'^+_{p\sigma}c'_{p'\sigma}, \qquad (27)$$

where ν represents the number of couplings between neighboring blocks. In Figure 1 $\nu = 3$. The last renormalization group equation is readily obtained:

$$t' = \nu\lambda^2 t. \qquad (28)$$

Up to now, we have given a general discussion of the conditions under which no proliferation of couplings results from the application of the BRG method to nonpartite lattice. Because on the border of nonpartite lattice block there is only one type of site, the above procedures can be extended to other lattices with different dimensions or blocks.

2.3. STATE SELECTIONS

After deriving the conditions for the renormalization group equations, the next task is to select states that satisfy these conditions. At this stage the symmetry properties of the lattice play an important role. From Eqs. (23) and (24) it can be easily seen that if we assume the particle number in the state $|0\rangle'$ to be $N_e - 1$ then in $|\uparrow\rangle'$, $|\downarrow\rangle'$, and $|\Uparrow\rangle'$ there should be N_e, N_e, and $N_e + 1$ particles, respec-

tively. Moreover, if the spin in $|0\rangle'$ is S_z, the spins for $|\uparrow\rangle'$, $|\downarrow\rangle'$, and $|\uparrow\downarrow\rangle'$ should be $S_z + 1/2$, $S_z - 1/2$, and S_z. The total electron number N_e and the spin S_z for each block are good quantum numbers because their corresponding operators commute with the Hubbard Hamiltonian. So, when we diagonalize the Hubbard Hamiltonian of the selected block we keep N_e and S_z fixed to be $(N_e - 1, S_z)$, $(N_e, S_z + 1/2)$, $(N_e, S_z - 1/2)$, and $(N_e + 1, S_z)$ respectively.

Thus, we obtain four groups of eigenenergies and eigenstates corresponding to the above quantum numbers. From each group, we select the lowest-energy state to form the final required four states. It should be mentioned that the lowest-energy state has to be selected according to definite special symmetry considerations, which shall be discussed in the next paragraph. To obtain the insulating to conducting gap, which is defined to be the energy difference between extracting one electron from the system and adding one electron to it, N_e is selected to be equal to N_s. For S_z, we choose it to be zero to make the block have the same spin property as the one site. So, now, the renormalized lattice will be composed of N/n_s renormalized "sites" with N/n_s "particles."

Instead of forcing the above conserved quantities upon the selected states in analogy to the one-site properties in a consistent way, here we get them directly from the no-coupling-proliferation conditions. λ does not depend on σ in Eq. (25); this can be guaranteed by the particle–hole symmetry, which means that only in half-filled lattice can the renormalized Hamiltonian have exactly the same form as the original one [37]. Moreover, the irrelevance of λ with respect to the border site $i^{(p,b)}$ can be shown by requiring the selected states to belong to the same irreducible representation of the spatial group of the lattice. For the triangular lattice with hexagonal blocks, the Hamiltonian is invariant under C_{6v} [38]. So, if we choose the same 1-D irreducible representation of the group C_{6v} for $|0\rangle'$, $|\uparrow\rangle'$, $|\downarrow\rangle'$, and $|\uparrow\downarrow\rangle'$ the conditions can be satisfied.

3. Computational Study of the Hubbard Model for an Ordered Lattice

The insulating gap (or charge gap) Δ_g [11] and the ground-state energy per site E_g for the half-filled Hubbard model on a triangular lattice with hexagonal blocks can be written as

$$\Delta_g = E(N_e) + E(N_e + 1) - 2E(N_e) = \lim_{n \to \infty} U^{(n)} \quad (29)$$

and

$$E_g = \lim_{n \to \infty} \frac{K^{(n)} + \dfrac{U^{(n)}}{4}}{7^n} + \frac{U}{2}, \quad (30)$$

where $E(N_e)$ represents the lowest energy of the system with N_e electrons, n denotes the number of iterations in the renormalization equations, and $U^{(n)}$ is the generalization to nth iterations of Eq. (15). The metal–insulator transition for this lattice can be examined by considering the scaled energy gap Δ_g/t as a function of U/t. If the insulating gap disappears the system exhibits metallic behavior. Otherwise, it is insulating.

Figure 2 shows the numerical results for the scaled gap Δ_g/t as a function of U/t. There is a first-order phase transition at $(U/t)_c \approx 12.5$. This finding is different from the case of half-filled square lattice, where an insulating gap exists for arbitrarily small values of U/t. This is because there is a perfect nesting of the Fermi surface on a square lattice, which makes the model unstable toward antiferromagnetism as soon as a nonzero U is
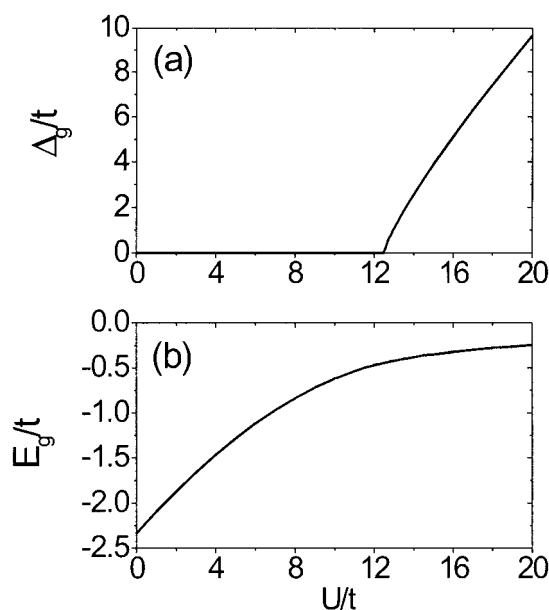
FIGURE 2. *U/t* The dependence of (a) the insulating gap Δ_g and (b) the ground-state energy per site E_g on the ratio, *U/t*, of the charging energy and the exchange coupling.

turned on, driving the system to an insulating state.

On the triangular lattice, for the lack of perfect nesting, metal–insulator transition takes place at a finite value of U/t. But, because there is no exact solution to the 2-D Hubbard model, there are still controversies upon the exact value for this critical point. The situation becomes more complicated and subtle because of the frustrations inherent in the triangular lattice, which may induce a nontrivial competitions among different magnetic phases. In the Hartree–Fock calculations by Krishnamurthy et al. [39, 40] they found that for small U/t the system is a paramagnetic metal that turns to a metal with incommensurate spiral spin-density wave at $(U/t)_{c1} = 3.97$. Two successive first-order phase transitions occur at $(U/t)_{c2} = 4.45$: A semimetallic linear spin-density wave is stabilized and a first-order metal–insulator transition to an antiferromagnetic insulator occurs at $(U/t)_{c3} = 5.27$. Capone et al. [41] obtained qualitatively similar phase transitions by using the Kotliar–Ruckenstein slave–boson technique, that is, the weak-coupling paramagnetic metal continuously evolves into a spiral metal at $(U/t)_{c1} = 6.68$, which crosses the linearly polarized spin-density-wave ground state at $(U/t)_{c2} = 6.84$. The latter phase undergo a further first-order transition toward an antiferromagnetic insulator at $(U/t)_{c3} = 7.68$. The exact diagonalization results exhibit a first-order transition between the paramagnetic metal and the antiferromagnetic insulator at $(U/t)_c = 12.07$, without intermediate "exotic" phases [42]. Our results for the critical value of $(U/t)_c \approx 12.5$ for the metal–insulator transition and the ground-state energy as a function of U/t are in agreement with results obtained by the exact diagonalization method [42].

All the above work is based upon the BRG method with hexagonal blocks. For comparisons, the results obtained by triangular blocks are presented in Figure 3, denoted by triangular–triangular, from which we can easily see the difference between the two RG schemes. For example, the critical point in the triangular–block scheme is 9.8 instead of 12.5 for the hexagonal–block one. The larger the block size, the more accurate are the results. But, to use larger blocks requires much more computation time. As a compromise between these two conflicting factors, i.e., block size and computer resources, we here put forward a multistaged block renormalization group method (MBRG). It is based upon the following considerations:
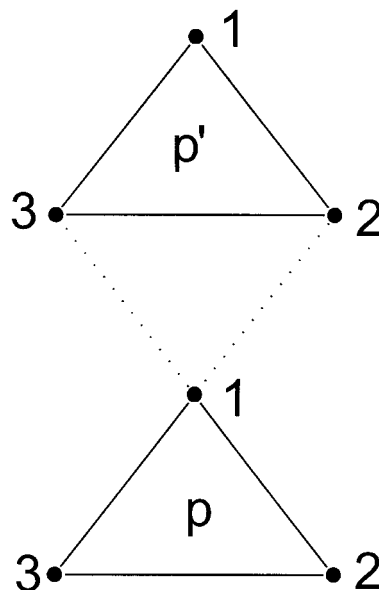

FIGURE 3. Schematic diagram of the triangular lattice with triangular blocks for use in the RG method.

1. The perturbative parameter for the RG method is t/U.
2. Following the flow of the RG equations, t/U will become smaller.
3. To choose larger block size will lead to smaller effective t/U after renormalizing the block to one site.

Thus, as the renormalization iterations go on, we may decrease the block size for renormalization. In our case we use the hexagonal block in the first step of the BRG method to get an effective Hamiltonian. Then, the triangular block is used in the following BRG steps. The critical value obtained in this way is $(U/t)_c = 11.3$, more accurate than 9.8 obtained from the RG method with only triangular blocks. To obtain more accurate results, we can also use hexagonal blocks in more than one step from the beginning, for example, in the first two or three steps. Although the result calculated with this method is not as accurate as that got by using hexagonal blocks in normal BRG, it still is an improvement compared to the normal triangular–block BRG. If we use hexagonal blocks in MBRG for more initial steps instead of only one step in our calculations, the accuracy of the results should be improved more and of course the calculations will be more intensive. Thus, this provides a satisfactory balance between accuracy and computation time.
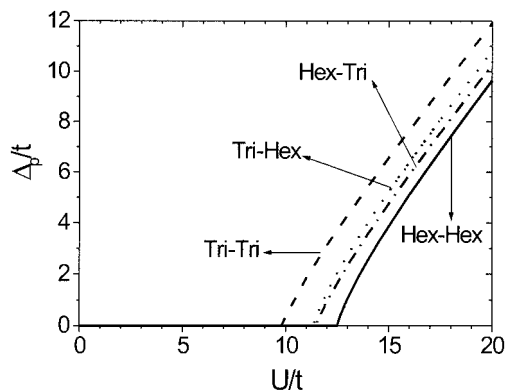
FIGURE 4. Comparisons of the U/t dependence of the insulating gap for triangular (Tri) lattice with different renormalization schemes. Dotted line (Tri–Hex): The lattice is first mapped onto an effective lattice with triangular block (Tri) and then renormalized with hexagonal blocks (Hex). The notations Hex–Hex (solid line), Hex–Tri (dotted-broken line), and Tri–Tri (broken line) have a corresponding meaning.

From Figure 4 it is also interesting to note that if we reverse the stage order, namely, using the triangular block first and then the hexagonal block, the accuracy of the results will be decreased. This is consistent with the above analysis that the first few steps should have the most important contributions to the final results.

The idea of MBRG can be useful in the study of disordered systems, which will be discussed in the following section.

4. Computational Results for Disordered Lattices Using the Hubbard Model

A physically realistic description of a lattice of QDs requires the introduction of the role of disorder. Here, we examine fluctuations in the two parameters of the ideal Hubbard model. These are the variations in the dot–dot coupling t that are due to both packing and size fluctuations and the variations in U that are essentially due only to size fluctuations. In principle, these parameters can vary from site to site but to apply a renormalization scheme we must first divide the infinite lattice into equivalent cells such that, in each cell, the disorder follows the same pattern. This can be regarded to be periodic boundary conditions for the cells. These cells do not necessarily coincide with the fundamental cells of the lattice

and can have any size. Then, we solve the one-cell system exactly and thus obtain an effective Hamiltonian for the cell and cell–cell interactions. Each cell can now be treated as a site. Because of the periodic boundary conditions the problem is thereby reduced to a renormalized ideal lattice, free of disorder. Then, we can use the usual BRG method upon the renormalized new lattice.

The above procedure is similar to the MBRG method mentioned at the end of the last section. The only difference is that we have a disordered cell in the first renormalization stage. In the following, we will first discuss disorder in t.

4.1. DOT–DOT COUPLING DISORDER

To simplify the calculations, the elementary cells (which are disordered) are chosen to be hexagonal blocks with C_{6v} symmetry. The detailed configuration is shown in Figure 5, in which the hopping terms between boundary sites are proportional to t and inside the cell proportional to t'. The corresponding Hamiltonian for the cell now becomes

$$H_p = -t \sum_{\langle i(p), j(p)\rangle=1,\sigma}^{6} [c_{i(p)\sigma}^{+} c_{j(p)\sigma} + \text{H.c.}]$$
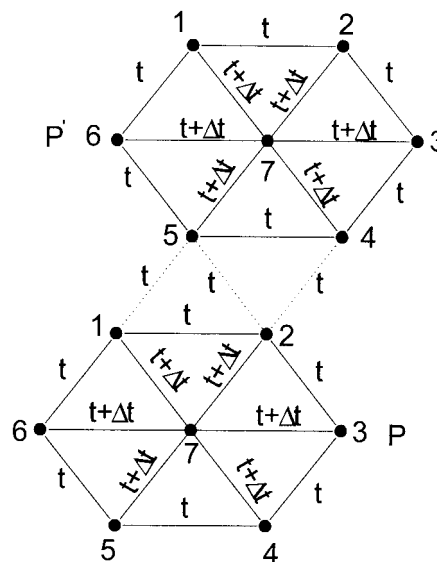

FIGURE 5. t and $t + \Delta t$ represent the hopping interaction between different sites connected by solid lines for interblock coupling and dotted lines for intrablock coupling.
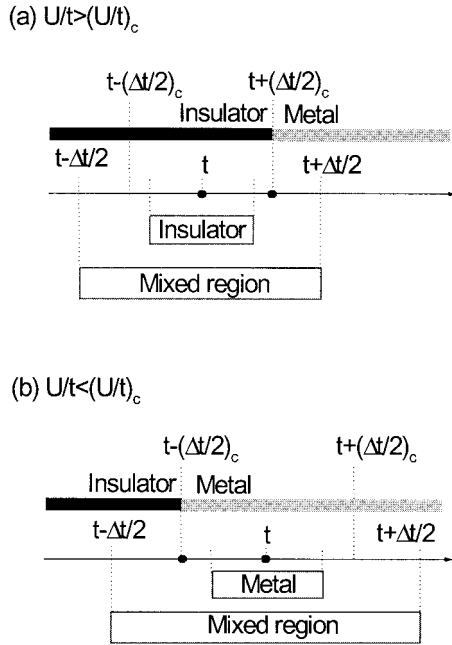
(a) $U/t > (U/t)_c$

(b) $U/t < (U/t)_c$

FIGURE 6. Diagramatic summary of the relation between the state of the system and fluctuations in the exchange coupling. Depending upon whether $[t - \Delta t/2, t + \Delta t/2]$ is a subset of $[t - (\Delta t)_c, t + (\Delta t)_c]$ or not, the system is in a definite phase or is mixed. (a) For higher charging energy when the definite phase is insulating. (b) For lower charging energy. $(U/t)_c$ is the boundary between insulating and metallic phases for the ordered lattice.

$$- t' \sum_{\langle 7(p), j(p) \rangle = 1, \sigma}^{6} [c_{7(p)\sigma}^{+} c_{j(p)\sigma} + \text{H.c.}]$$

$$+ U \sum_{i^{(p)}} n_{i^{(p)}\uparrow} n_{i^{(p)}\downarrow} - \frac{U}{2} \sum_{i^{(p)}} (n_{i^{(p)}\uparrow} + n_{i^{(p)}\downarrow}). \quad (31)$$

The probability distribution function for t' is taken to be

$$P(t') = \begin{cases} 0, & (t' > t + \Delta t/2 \text{ or } t' < t - \Delta t/2) \\ \dfrac{1}{\Delta t}, & (t - \Delta t/2 < t' < t + \Delta t/2), \end{cases} \quad (32)$$

in which $\Delta t (>0)$ denotes the range of the fluctuation in the coupling strength.

We discuss the results for two regimes depending on the onset of the insulating phase in the ordered array, that is, the two regimes correspond to whether $U/t > (U/t)_c$ or $U/t < (U/t)_c$.

In the absence of disorder (i.e., $\Delta t = 0$) the range $U/t > (U/t)_c$ corresponds to the insulating phase.

Then, as Δt increases upward from zero the coupling strength for the electrons to hop to the neighboring sites increases because $t' = t + \Delta t$, which the insulating gap Δ_p will decrease. At some critical value of $(\Delta t)_c$ Δ_p will drop suddenly to zero and the insulating state crosses into a metallic phase. This process is schematically shown in Figure 6(a). At the other half of the range of variation of the hopping term, i.e., $t' = t - \Delta t$, the system will stay in the insulating state for any (positive) value of Δt. Because the fluctuating hopping term t' varies uniformly over the range $t - \Delta t$ to $t + \Delta t$ it follows that the system will be in a mixed region whenever $\Delta t > (\Delta t)_c$. Here, "mixed" means that the system is either in a metallic state or in a insulating state, depending on the local value of the fluctuation. If we imagine dividing the infinite lattice into nonoverlapping domains, then the above discussions can be applied in each domain separately. We would then find that some domains are localized in an insulating state while others are delocalized and are in a metallic state. This provides a quantitative phase diagram as shown in Figure 7. Specifically, it verifies the notion of domain-localized states [33] as shown in the phase diagrams in [34].

Recently, clear experimental evidence has been obtained for domain localization. The evidence is of two kinds, the first structural. For an array of QDs, both the surface potential and surface topographical coverage could be simultaneously determined [7]. While the packing was imaged to be completely regular and ordered, the surface potential exhibited clear domain structure. The second experiment is a transport measurement [8, 32, 43]. This does not image the domain but provides evidence for their role in conduction at below room temperatures.
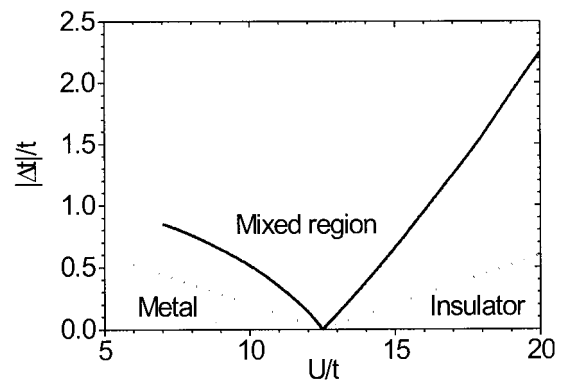

FIGURE 7. Phase diagram for the triangular lattice with coupling disorder given in Figure 5 (solid line).
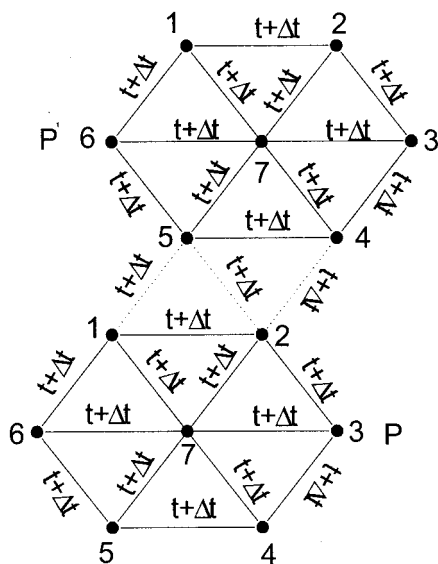
FIGURE 8. Same as in Figure 5 but for couplings that are all deviant in the same manner.

$$\frac{U/t}{1 + \Delta t/t} = (U/t)_c, \quad (U/t > (U/t)_c), \quad (33)$$

$$\frac{U/t}{1 - \Delta t/t} = (U/t)_c, \quad (U/t < (U/t)_c). \quad (34)$$

This leads to an explicit equation for the phase boundary

$$|U/t - (U/t)_c| = (\Delta t/t)_c. \quad (35)$$

This boundary is also shown in Figure 7 (dotted line), from which we can see that the general structure is similar to that found in the last paragraph but that the mixed region is much larger. This is understandable because the present case introduces a change in the mean coupling strength.

For the complementary range, where $U/t > (U/t)_c$, the discussions can be carried out in a similar way. The only difference is that we have to start from the metallic state when $\Delta t = 0$. Then, at some critical point with $t' = t + (\Delta t)_c$ the system will cross to an insulating state, which equally leads to a mixed region in the phase diagram. Figure 6(b) summarizes the discussion. From the phase diagram in Figure 7, one sees that the insulating and metallic states are influenced by the disorder to about the same extent. For example, if both states have the same distance $|U/t - (U/t)_c|$ to the critical point $(U/t)_c$ about the same value of the disorder $(\Delta t)_c$ can take them to the mixed region. It is also interesting to note that because one can, to some extent, control the disorder it may be possible to decide how far the state is from the critical state at $U/t = (U/t)_c$.

In all the above discussions, we considered only the special kind of disorder, which preserve the C_{6v} symmetry of the triangular lattice. Keeping this symmetry is necessary to reduce the computation time. Finally, we consider a disorder that has the aqdvantage that it allows for an analytic solution for the phase boundary. As was shown, the metal–insulator transition in the Hubbard model only depends on the ratio U/t. So, if all the hopping terms fluctuate in the same direction and by the same amount, which is demonstrated in Figure 8, then the critical disorder $(\Delta t)_c$ should satisfy

4.2. FLUCTUATIONS IN THE CHARGING ENERGY

Here, too, we consider only disorder of a special kind. The pattern of the allowed variations in the charging energy is shown in Figure 9, namely, the fluctuations of U are allowed only in the central site of the cell. Thus, the C_{6v} symmetry is preserved. The new Hamiltonian for the cell now becomes
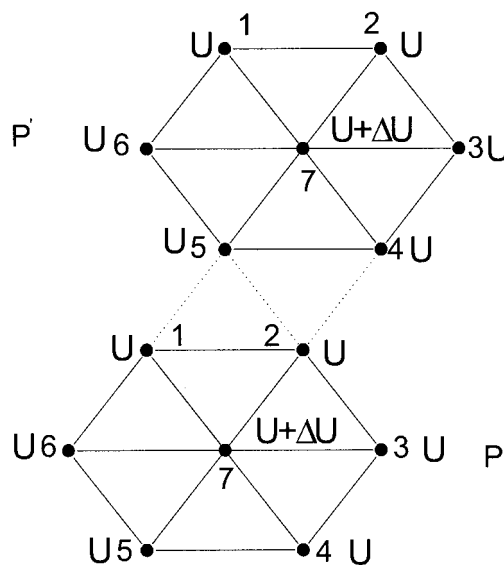

FIGURE 9. Cells showing the central site with a different charging energy. The same as in Figure 5 but for U.
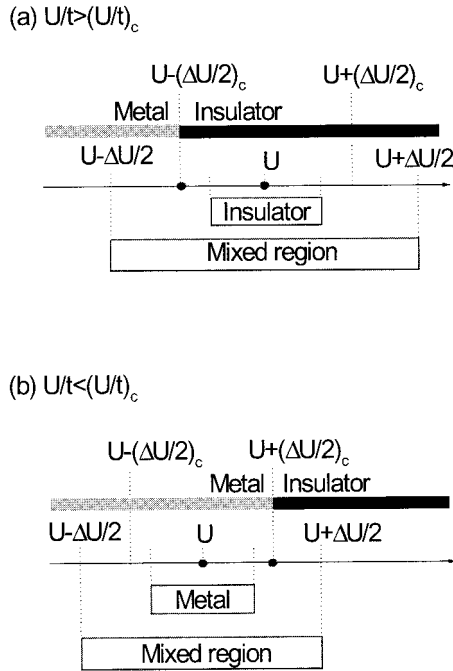
FIGURE 10. Diagramatic summary of the relationship between the state of the system and fluctuations in the charging energy. A similar representation to that shown in Figure 6.

$$H_p = -t \sum_{\langle i^{(p)}, j^{(p)} \rangle = 1, \sigma}^{7} [c_{i^{(p)}\sigma}^{+} c_{j^{(p)}\sigma} + \text{H.c.}]$$

$$+ U \sum_{i^{(p)}=1}^{6} n_{i^{(p)}\uparrow} n_{i^{(p)}\downarrow} - \frac{U}{4} \sum_{i^{p}=1}^{6} (n_{i^{(p)}\uparrow} + n_{i^{(p)}\downarrow})$$

$$+ (U') n_{7^{(p)}\uparrow} n_{7^{(p)}\downarrow} - \frac{U'}{4} (n_{7^{(p)}\uparrow} + n_{7^{(p)}\downarrow}). \quad (36)$$

The probability distribution function is given by

$$P(U')$$

$$= \begin{cases} 0, & (U' > U + \Delta U / 2 \text{ or } U' < U - \Delta U / 2) \\ \dfrac{1}{\Delta U}, & (U - \Delta U / 2 < U' < U + \Delta U / 2) \end{cases}.$$

$$(37)$$

Figure 10 demonstrates how to determine the critical value of $(\Delta U)_c$ as in Figure 6. The final phase diagram is presented in Figure 11. It is interesting to note the asymmetrical influence of site disorder upon the metallic and insulating states. The disorder-induced crossing of the insulating states to the mixed region is easier than that of the metallic
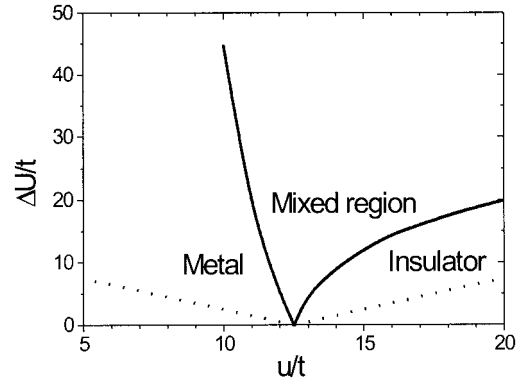

FIGURE 11. Phase diagram for the triangular lattice with site disorder given in Figure 9 (solid line) or the disorder (dotted line) shown in Figure 12.

states. This may reflect the second-order nature of the transition [34] out of the insulating phase to the domain-localized regime. It also implies that in the metallic phase it takes higher fluctuations in U to localize the electrons. It is interesting to speculate if this asymmetrical response to disorder can lead to hysteresis in the phase transition.

For this case, too, we can consider a caricature of disorder (Fig. 12), where all the sites fluctuate in the same manner. Now, the phase boundary is at

$$|U/t - (U/t)_c| = (\Delta U/t)_c,$$
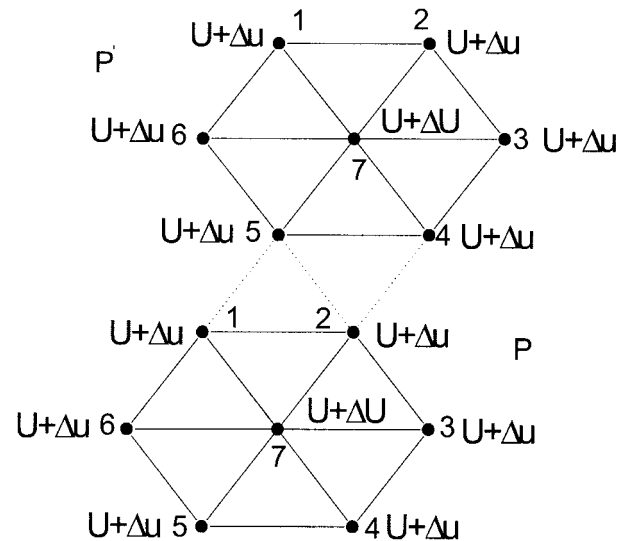
which is also shown in Figure 10.

FIGURE 12. Same as in Figure 8 but for the charging energies that are all deviant in the same manner.

5. Hubbard–Anderson Model

Besides the Mott MIT characterized by the charge gap, there is another kind of MIT caused by the site disorder, which is known as Anderson MIT. The mechanism underlying these two effects are different. In the insulating state of a half-filled lattice, for the former, one site tends to hold one electron because of the on-site repulsion, while for the latter the sites are expected to be doubly occupied instead. Hence, even in the weak coupling regime we can still have insulators, which are gapless and caused by site disorder. The combining effects of site disorder and electron–electron interaction are complicated. It has now become the heart of many interesting and unexplained phenomena in condensed matter physics. For example, where both disorder and interactions are crucial yet incompletely understood include the formation of local moments and the behavior of the susceptibility in doped semiconductors [44], the superconductor–insulator transition and universal conductivity in thin metallic films [45, 46], and the pinning of flux lines in type-II superconductors [47]. One of the most important physical quantities in the studying of Anderson MIT is the inverse participation rate, which measures the extent of the electron localization and delocalization in the system. What we will do here is to investigate the influence of electron–electron interactions on the localized properties of 2-D electrons in disordered systems.

5.1. APPROACHES

The Hamiltonian for the Anderson–Hubbard model can be written as

$$H = -t \sum_{\langle i,j \rangle, \sigma} [c_{i\sigma}^+ c_{j\sigma} + \text{H.c.}] + U \sum_i \left(n_{i\uparrow} - \frac{1}{2} \right)\left(n_{i\downarrow} - \frac{1}{2} \right)$$
$$- \sum_i \varepsilon_i (n_{i\uparrow} + n_{i\downarrow}), \quad (38)$$

where ε_i measures the fluctuation of the site energies. It is assumed that ε_i follows Gaussian distribution with the width to be W, i.e.,

$$P(\varepsilon_i) = \frac{1}{\sqrt{2\pi W}} e^{-[(\varepsilon_i - \bar{\varepsilon})^2 / 2W]}, \quad (39)$$

in which the bar over ε means its average value. Initially, we use $\bar{\varepsilon} = 0$.

Because there is no exact particle–hole symmetry anymore once the disorder is introduced into the Hamiltonian, the parameters t, U, and ε_i have to be renormalized on average. In detail, let us use α and β to be the block indice. Then, for one block α we can have

$$U^\alpha = E_1^\alpha + E_2^\alpha - 2E_3^\alpha, \quad (40)$$

$$\varepsilon^\alpha = E_2^\alpha - E_1^\alpha. \quad (41)$$

Normally, the new energies ε^α does not obey a Gaussian distribution anymore. To itinerate the RG [48], we adopt the following procedures:

1. ε^α is forced back into a Gaussian distribution with the new width
$$W' = \overline{(\varepsilon^\alpha)^2} - (\overline{\varepsilon^\alpha})^2. \quad (42)$$

 The new Gaussian is not centered at zero because there will be a constant shift due to the electron interactions. But, we can still take it to be zero by formally introducing the chemical potential.

2. U^α is forced back to be constant:
$$U' = \overline{U^\alpha}. \quad (43)$$

3. To get the renormalized hopping term, we will have to consider all the possible nonzero average values of the coupling between the block states. For two neighboring blocks, there are four possibilities:

$$t_1^{\alpha\beta} = t\langle \uparrow {}^\alpha 0^\beta | \sum_{\langle \alpha i, \beta j \rangle, \sigma} [c_{\alpha i\sigma}^+ c_{\beta j\sigma}] | \uparrow {}^\beta 0^\alpha \rangle, \quad (44)$$

$$t_2^{\alpha\beta} = t\langle \uparrow\downarrow {}^\alpha 0^\beta | \sum_{\langle \alpha i, \beta j \rangle, \sigma} [c_{\alpha i\sigma}^+ c_{\beta j\sigma}] | \uparrow {}^\beta \downarrow {}^\alpha \rangle, \quad (45)$$

$$t_3^{\alpha\beta} = t\langle \uparrow {}^\alpha \downarrow {}^\beta | \sum_{\langle \alpha i, \beta j \rangle, \sigma} [c_{\alpha i\sigma}^+ c_{\beta j\sigma}] | \uparrow\downarrow {}^\beta 0^\alpha \rangle, \quad (46)$$

$$t_4^{\alpha\beta} = t\langle \uparrow\downarrow {}^\alpha \downarrow {}^\beta | \sum_{\langle \alpha i, \beta j \rangle, \sigma} [c_{\alpha i\sigma}^+ c_{\beta j\sigma}] | \uparrow\downarrow {}^\beta \downarrow {}^\alpha \rangle. \quad (47)$$

We also force the distribution of $t^{\alpha\beta}$ into a Gaussian with mean

$$t' = \overline{t_i^{\alpha\beta}} \quad (48)$$

and width

$$t_2' = \overline{(t_i^{\alpha\beta})^2} - (\overline{t_i^{\alpha\beta}})^2. \quad (49)$$

In principle, to use more blocks for averaging is always desirable. In our work, we use seven-unit blocks, which themselves form a hexagonal block.

5.2. RESULTS

When the noninteracting electrons are confined to two spatial dimensions in a disordered environment, it has been established that all the electronic states will be localized and the system will be an insulator. This result is based upon the scaling theory and then corroborated by RG methods. But, the situation drastically changes when the electron interactions are considered, which is likely to play an important role to explain the recently found 2-D MIT in experiments. Until now, we have shown how Mott MIT happens in the Hubbard model with the BRG method. In this section, we will further demonstrate the competition effect between disorders and electron interactions with the procedures developed above. What we are going to do here is show how the electron interactions can influence their localization, which is the principle mechanism for the Anderson insulator.

The localization feature can be exposed by the inverse participation rate (IPR) ξ, defined as

$$\xi^{(4)} = \frac{N_e}{\sum_i |\langle\psi|(\hat{n}_{i\uparrow} + \hat{n}_{i\downarrow})|\psi\rangle|^4}, \tag{50}$$

where $\hat{n}_{i\sigma} = c^+_{i\sigma}c_{i\sigma}$ is the number operator, N_e is the total number of the electrons, which is equal to the site number N_s, and ψ is the system wave function. For totally localized electronic states in the half-filled system, half of the sites have $\langle\psi|\hat{n}_i|\psi\rangle = 2$. Then, we can get

$$\xi^{(4)}_{localize} = \frac{N_e}{8N_s} = 0.125. \tag{51}$$

On the other hand, when the electron is totally delocalized, the average number of electrons per site should be $\langle\psi|\hat{n}_i|\psi\rangle = 1$. Then,

$$\xi^{(4)}_{localize} = \frac{N_e}{N_s} = 1. \tag{52}$$

Hence, the IPR $\xi^{(4)}$ will vary in the above two extreme values, namely, $0.125 \leq \xi^{(4)} \leq 1$. If more general definition for the IPR is introduced, we can have

$$\xi^{(k)} = \frac{N_e}{\sum_i |\langle\psi|\hat{n}_i|\psi\rangle|^k}, \tag{53}$$

which might be useful to study the scaling properties of the electronic transport properties. In the same way as above, it can be easily shown that

$$\frac{1}{2^{k-1}} \leq \xi^{(k)} \leq 1. \tag{54}$$

As one trivial case, $\xi^{(1)}$ is always to be 1.

In Figure 13, the variation of $\xi^{(k)}$ against the electron interaction U is presented for fixed magnitude of disorder. It is easy to see that all the curves have the same trend when electron–electron interaction increases from zero. In general, there are three stages:

1. When U is small ($U < W$), electron–electron interactions tend to hinder the electron localizations resulting from the disorders. This is consistent with the findings by Ma [48]. It is understandable when the following fact is considered: The on-site electron repulsions will make the Anderson localizations with two electrons on one site more difficult. Even if the two electrons sit on one site, the interaction between them will drive their wave functions more extended or more delocalized.

2. When U is much larger than w, the similar phenomenon as above takes place also. But, the electron now is totally delocalized, with each site having one electron on average and no double occupancy is present. There is a limiting case with $U \rightarrow \infty$, where each electron will be localized on one site. Because the magnetic properties of the system are not investigated in this work, we will not consider this kind of localization here.

3. In the medium of U, where the magnitudes of the interactions and disorders are competitive, there is a complicated dependence of the IPR upon the electron–electron interactions. First, the electron–electron interactions will enhance the electron localizations. Then, after a flat platform with all the electrons localized, the electrons will become totally delocalized when U is beyond a transition point, from which starts the emergence of Mott insulating states as shown in Figure 13.

6. Conclusions

A practical renormalization method for an array described by a Hubbard Hamiltonian has been presented. The method is especially suited for getting low excited states. An application demonstrating the identification of a first-order metal–insulator transition has been discussed in detail. MBRG is put forward to improve the accuracy of the results without requiring much more computation time. We also used the idea of MBRG to study the Hubbard model with disorder, which is an essential aspect of QDs. Calculations including disorder in the exchange coupling t and charging energy U were carried out. From the $U/t - (\Delta t/t)_c$ phase diagram, a mixed region of insulating and metallic domains is found and is discussed in detail. The site–energy disorder considered in the Anderson–Hubbard model is also discussed from the viewpoint of electron–electron interaction disorder competitions. Work is underway to apply the MBRG method to the computations of transport properties of lattices of QDs.
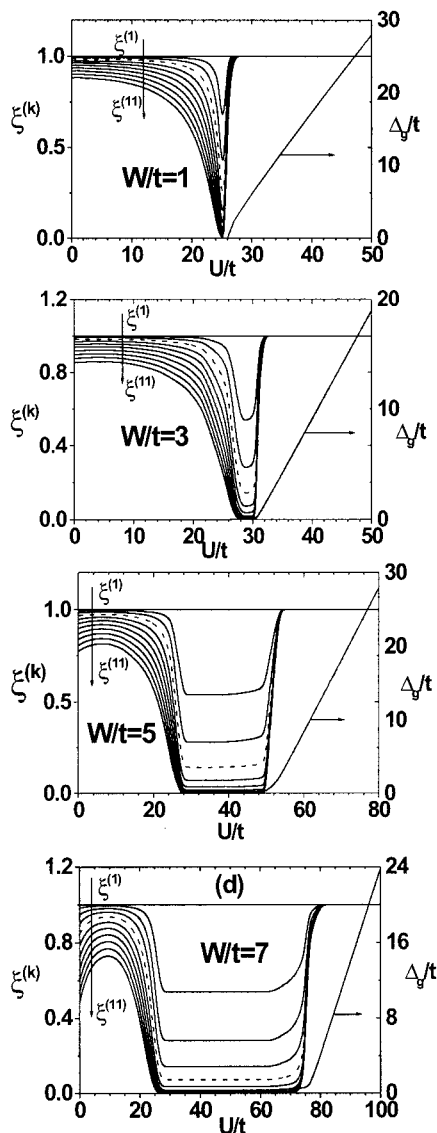
FIGURE 13. Influence of electron–electron interactions upon the IPR (left axis) and the charge gas (right axis) when the distribution width of the site–energy disorder is (a) $W/t = 1$, (b) $W/t = 3$, (c) $W/t = 5$, and (d) $W/t = 7$. The broken line represents the conventional IPR $\xi^{(4)}$ while the others represents the generalized IPR $\xi^{(k)}(k \neq 4)$.

In general, when U is small the system is a gapless Anderson insulator and when U is big the system is a gap Mott insulator. In the middle region of U, the system is gapless and displays a complex competition between the disorders and interactions. Moreover, as we increase the disorders, this middle region becomes wider, which clearly exhibits how an Anderson insulating state evolves into a Mott insulating state as the electron correlations increases.

References

1. Markovich, G.; Collier, C. P.; Henrichs, S. E.; Remacle, F.; Levine, R. D.; Heath, J. R. Acc Chem Res 1999, 32, 415–423.

2. Beverly, K. C.; Sample, J. L.; Sampaio, J. F.; Remacle, F.; Heath, J. R.; Levine, R. D. Proc Natl Acad Sci USA 2002, 99, 6456.

3. Bennett, C. H.; DiVincenzo, D. P. Nature 2000, 404, 247–255; Burkard, G.; Loss, D.; DiVincenzo, D. P. Phys Rev B 1999, 59, 2070–2078; Loss, D.; DiVincenzo, D. P. Phys Rev A 1998, 57, 120–126.

4. Kastner, M. A. Phys Today 1993, 46, 24–31; Ashoori, R. C. Nature 1996, 379, 413–419; Banin, U.; Cao, Y. W.; Katz, D.; Millo, O. Nature 1999, 400, 542–544.

5. Head-Gordon, M. J Phys Chem 1996, 100, 13213.

6. Remacle, F.; Levine, R. D. J Am Chem Soc 2000, 122, 4084; Remacle, F.; Levine, R. D. J Phys Chem A 2000, 104, 10435.

7. Sample, J. L.; Berverly, K. C.; Chaudhari, P. R.; Remacle, F.; Heath, J. R.; Levine, R. D. Adv Mater 2002, 14, 124.

8. Beverly, K. C.; Sampaio, J. F.; Heath, J. R. J Phys Chem 2002, 106, 2131.

9. Hubbard, J. Proc Roy Soc Lond A 1963, 276, 238; Hubbard, J. Proc Roy Soc Lond A 1964, 277, 237; Hubbard, J. Proc Roy Soc Lond A 1964, 281, 401.

10. Lieb, E. H. arXiv: cond-mat/9311033; 1993; Tasaki, H. arXiv: cond-mat/9512169; 1997; Tasaki, H. arXiv: cond-mat/9712219; 1997, and references therein arxiv.org e-print archive, Los Alamos, NM.

11. Lieb, E.; Wu, F. Phys Rev Lett 1968, 20, 1445.

12. Senechal, D.; Perez, D.; Pioro-Ladriere, M. Phys Rev Lett 2000, 84, 522.

13. White, S. R.; Scalapino, D. J.; Sugar, R. L.; Loh, E. Y. Jr.; Gubernatis, J. E.; Scalettar, R. T. Phys Rev B 1989, 40, 506.

14. Penn, D. Phys Rev 1966, 142, 350.

15. Tahir-Kheli, R.; Jarrett, H. Phys Rev 1968, 180, 544; Roth, L. Phys Lett 1981, 20, 1431; Kishore, R.; Joshi, S. Phys Rev 1969, 186, 484; Arai, T.; Parinellok, M. Phys Rev Lett 1971, 27, 1226.

16. Cyrot, M. J Phys Paris 1972, 33, 125; Kimball, J.; Schriieffer, J. R. Int Conf Magnet 1971; Cyrot, M. Phys Rev Lett 1970, 25, 871; Cyrot, M.; Lacour-Gayet, P. J Phys C 1974, 7, 400.

17. Gutzwiller, M. C. Phys Rev A 1965, 137, 1726; Gutzwiller, M. C. Phys Rev Lett 1963, 10, 159; Langer, W.; Plischke, M.; Mattis, D. Phys Rev Lett 1969, 23, 149; Kaplan, T.; Bari, R. J Appl Phys 1970, 41, 875; Brinkman, W.; Rice, T. M. Phys Rev B 1970, 2, 4302; Chao, K. A. Phys Rev B 1971, 4, 4034.

18. Harris, A. B.; Lange, R. V. Phys Rev 1967, 157, 295; Hubbard, J. Proc Roy Soc Lond A 1966, 296, 100; Kanamori, J. Progr Theor Phys Kyoto 1963, 30, 275; Esterling, D.; Lange, R. V. Rev Mod Phys 1968, 40, 796.

19. White, S. R. Phys Rev Lett 1992, 69, 2863; White, S. R. Phys Rev B 1993, 48, 10345.

20. Tokuyasu, T.; Kamal, M.; Murthy, G. Phys Rev Lett 1993, 71, 4202.

21. Murthy, G.; Kais, S. Chem Phys Lett 1998, 290, 199.

22. Hirsch, J. E. Phys Rev B 1979, 20, 3907; Hirsch, J. E. Phys Rev B 1980, 22, 5259.

23. Dasgupta, C.; Pfeuty, P. J Phys C 1981, 14, 717; Jullien, R.; Pfeuty, P.; Fields, J. N.; Doniach, S. Phys Rev B 1978, 18, 3568.

24. Perez-Conde, J.; Pfeuty, P. Phys Rev B 1993, 47, 856; Vanderzande, C. J Phys A Math Gen 1985, 18, 889.

25. Bhattacharyya, B.; Sil, S. Phys Condens Matter 1999, 11, 3513; Bhattacharyya, B.; Sil, S. Phys Lett A 1993, 180, 299.

26. Mott, N. F. Metal–Insulator Transitions; Taylor and Francis: London, 1990.

27. Wang, J. X.; Kais, S.; Levine, R. D. Int J Mol Sci 2002, 3, 4–16.

28. Wang, J. X.; Kais, S. Phys Rev B 2002, 66, 081101.

29. Remacle, F.; Collier, C. P.; Heath, J. R.; Levine, R. D. Chem Phys Lett 1998, 291, 453.

30. Remacle, F.; Collier, C. P.; Markovitch, G.; Heath, J. R.; Banin, U.; Levine, R. D. J Phys Chem B 1998, 102, 7727.

31. Remacle, F.; Levine, R. D. Chem Phys Chem 2001, 2, 20.

32. Remacle, F.; Beverly, K. C.; Heath, J. R.; Levine, R. D. J Phys Chem 2002, B106, 4116.

33. Remacle, F.; Levine, R. D. J Phys Chem B 2001, 105, 2153.

34. Remacle, F.; Levine, R. D. Proc Natl Acad Sci USA 2000, 97, 553; Remacle, F.; Levine, R. D. Chem Phys Chem 2001, 2, 20.

35. Burkhardt, T. W.; van Leeuwen, J. M. J., eds. Topics in Current Physics, Real-Space Renormalization; Springer-Verlag: New York, 1982.

36. Imada, M.; Fujimori, A.; Tokura, Y. Rev Mod Phys 1998, 70, 39.

37. Bhattacharyya, B.; Sil, S. Phys Lett A 1993, 180, 299.

38. Boardman, A. D.; O'Connor, E.; Young, P. A. Symmetry and Its Application in Science; John Wiley & Sons: New York, 1973.

39. Krishnamurthy, H. R.; Jayaprakash, C.; Sarker, S.; Senzel, W. Phys Rev Lett 1990, 64, 950.

40. Jayaprakash, C.; Krishnamurthy, H. R.; Sarker, S.; Wenzel, W. Europhys Lett 1991, 15, 625.

41. Capone, M.; Capriotti, L.; Becca, F.; Caprara, S. Phys Rev B 2001, 63, 0854104.

42. Brinkman, W. F.; Rice, T. M. Phys Rev B 1970, 2, 4302.

43. Collier, C. P.; Saykally, R. J.; Shiang, J. J.; Henrichs, S. E.; Heath, J. R. Science 1997, 277, 1978.

44. Bhatt, R. N.; Lee, P. A. Phys Rev Lett 1982, 48, 344; Paalanen, M. A.; Graebner, J. E.; Nhatt, R. N.; Sachdev, S. Phys Rev Lett 1988, 61, 597.

45. Goldman, A. M.; Markovic, N. Phys Today 1998, 51, 39.

46. Fisher, M. P. A.; Weichman, P. B.; Grinstein, G.; Fisher, D. S. Phys Rev B 1989, 40, 546.

47. Blatter, G., et al. Rev Mod Phys 1994, 66, 1125.

48. Ma, M.; Halperin, B. I.; Lee, P. A. Phys Rev B 1986, 3136.